



# Theoretical Analysis of Diamond Mechanosynthesis. Part I. Stability of C<sub>2</sub> Mediated Growth of Nanocrystalline Diamond C(110) Surface

Jingping Peng, Robert A. Freitas Jr.,\* and Ralph C. Merkle

Zyvex Corp., 1321 North Plano Road, Richardson, Texas 75081, USA

A theoretical investigation of the chemical vapor deposition (CVD) growth on clean diamond C(110) surfaces from carbon dimer precursors shows that isolated deposited C<sub>2</sub> dimers appear stable at room temperature, but a second carbon dimer subsequently chemisorbed in close vicinity to the first can adopt one of 19 local energy minima, five of which require barriers >0.5 eV to reach the global minimum and, thus, constitute stabilized defects. Three chemisorbed C<sub>2</sub> dimers can adopt one of 35 local minimum energy structures, 10 of which are stable defects located in deep potential energy wells. The number of potential defects increases with the number of deposited carbon dimers, which suggests an isolated rather than clustered growth mechanism in CVD on bare diamond C(110). These results also provide information regarding outcomes of the misplacement of a carbon dimer and establish constraints on the required dimer-placement positional precision that would be needed to avoid the formation of stable defects during diamond surface growth.

**Keywords:** Acetylene, Carbon, CVD, Density Functional Theory, Diamond, Dicarbon, Dimer, Mechano-synthesis, Nanotechnology, Positional Control, VASP.

## 1. INTRODUCTION

Diamond synthesis by chemical vapor deposition (CVD) at pressures and temperatures where diamond is metastable with respect to graphite was first achieved in 1952–1953,<sup>1</sup> and this process continues to be of great practical utility.<sup>2</sup> Under customary laboratory CVD growth conditions, the diamond C(110) face is the fastest-growing plane<sup>3–6</sup> as evidenced, for example, by scanning electron microscopy studies showing that only the C(111) and C(100) facets are found to occur predominantly in polycrystalline diamond films.<sup>7</sup> For this reason, the C(110) face is considered the hardest to grow by conventional CVD techniques.<sup>7–10</sup> Wild et al.<sup>11</sup> reported the absence of the C(110) surface on CVD-grown polycrystalline diamond films despite their overall (110) bulk orientation. In contrast to the high-quality homoepitaxial diamond growth on a C(100) surface, relatively poor quality homoepitaxial diamonds are obtained on

the C(110) surface,<sup>7</sup> largely due to the presence of a nondiamond phase, numerous twins, stacking faults and other defects.<sup>12, 13</sup> Attempts to grow homoepitaxial films on the C(110) surfaces with a hot filament CVD reactor<sup>14</sup> and a microwave plasma-assisted CVD system<sup>15, 16</sup> have also failed to produce smooth surfaces, although microwave CVD has been used to grow single and double layers of C(110) diamond on Si substrates with a 2.5% CH<sub>4</sub>/97.5% H<sub>2</sub> vol. % gas mixture.<sup>17</sup> New methods for preparing atomically smooth C(110) surfaces would be welcome.

Various possible sequences<sup>18, 19</sup> of CVD diamond growth events on the monohydrogenated C(110)-H(1 × 1) diamond surface involving C<sub>2</sub>H<sub>2</sub> precursor have been described elsewhere.<sup>3, 25–28</sup> A theoretical analysis by Battaile et al.<sup>19</sup> concluded that the growth of C(110) is 2–10 times faster than the growth of C(111) at various C<sub>2</sub>H<sub>2</sub> concentrations, but growth at the highest C<sub>2</sub>H<sub>2</sub> concentrations (~0.2 torr) used in CVD produces an atomically rough C(110) surface.<sup>20</sup> Simulations<sup>19–21</sup> and experiments<sup>10, 22, 23</sup> show that C<sub>2</sub>H<sub>2</sub> is necessary to promote nucleation on C(110),

\*Author to whom correspondence should be addressed.

although D'Evelyn et al.<sup>24</sup> estimate the efficiency of conventional CVD diamond formation from  $C_2H_2$  alone to be only  $\sim 5\%$  of the value from  $CH_3$ .

C(110) surface growth by direct carbon dimer ( $C_2$ ) radical insertion has been explored theoretically, both in the case of growth on the H-terminated surface without hydrogen abstraction by way of insertion of  $C_2$  into C-H bonds on the surface,<sup>29, 30</sup> and also in the case of growth by deposition of  $C_2$  onto the clean C(110) surface.<sup>33</sup> Experimentally, Gruen et al.<sup>34</sup> found high deposition rates and good mechanical properties of ultra-nanocrystalline diamond films grown from carbon dimer ( $C_2$ ) precursors produced by  $C_{60}$  fragmentation in hydrogen-poor plasmas,<sup>29–32</sup> and there is evidence<sup>35</sup> that this growth proceeds mainly on the C(110) face.<sup>33</sup> Unlike the bare C(111)<sup>36</sup> and C(100)<sup>37</sup> surfaces which rapidly reconstruct, the clean C(110) diamond surface does not reconstruct even after annealing to  $>1300$  K,<sup>38</sup> as confirmed by both theoretical<sup>33, 39, 40</sup> and experimental<sup>38, 41</sup> results, allowing C(110) surface atoms to retain their original crystallographic orientations—including the presence of well-defined troughs arranged as staggered rows of carbon dimers on C(110).

This paper presents a computational and theoretical investigation of the gas-phase chemical vapor deposition growth and mechanosynthesis of clean diamond C(110) surfaces from carbon dimer precursors. In Part I, we provide a detailed atomic picture of the dimer-mediated surface chemistry during the gas-phase growth of diamond C(110) from  $C_2$  plasmas, and deduce some of the many possible stabilized defects that can be formed early in the dimer-mediated diamond growth process. These results provide information regarding outcomes of the misplacement of a carbon dimer and establish constraints on the required dimer-placement positional precision that would be needed to avoid the formation of stable defects during surface growth. Positional dimer placement for dimer growth of diamond has been proposed elsewhere<sup>42</sup> and is investigated theoretically in Part II.<sup>43</sup>

## 2. COMPUTATIONAL METHODS

All calculations were performed using plane wave-based density functional theory (DFT). The software for computation was the Vienna *ab initio* Simulation Package (VASP).<sup>44</sup> The generalized gradient approximation (GGA) using Perdew-Wang 91 (PW91) pseudopotentials generated with conventional local density approximation (LDA) reference configurations was utilized in the calculations. The energy cutoff of 211.29 eV for pseudopotential was adopted throughout. The criterion of energy convergence for SCF loop (optimizing wavefunction) was  $1 \times 10^{-5}$  eV, and the criterion for geometry optimization was  $1 \times 10^{-3}$  eV.

The clean diamond C(110) surface was modeled as a 4-layer carbon atom slab consisting of 96 carbon atoms and 24 hydrogen atoms (just fitting the unit cell of the computational system), with the bottom carbon layer saturated with

a layer of hydrogen atoms. The surface is a flat symmetric ( $1 \times 1$ ) structure with 2 troughs. The flat surface of the model was placed parallel to the  $xy$  ( $z = 0$ ) plane with the minimum  $z$  coordinate set to zero. The dimensions of the unit cell of the system (box dimensions) are 10.6840 Å in the  $x$  direction, 10.0835 Å in the  $y$  direction and 15.0000 Å in the  $z$  direction. Before calculating the stationary points of surface growth, the geometry of the surface model was fully optimized.

The stationary points were found by placing one or more carbon dimers on several selected initial positions within a trough on the dehydrogenated diamond C(110) surface model, then relaxing the system to the minimum energy structure. During the geometry optimization, the bottom layer of the four carbon layers and all terminating hydrogen atoms, a total of 48 atoms, were frozen. To estimate the barriers from a local minimum to the global minimum, the following approaches were used depending on the individual situation. Most often, the pertinent dimer of a local minimum was raised or lowered with a step size of 0.05 or 0.1 Å along the  $z$  axis (vertically). At each step, the  $z$  coordinate of both ends or one end of the relevant dimer was fixed and the system was then relaxed. If a climax occurred along the path, then the fixed  $z$  coordinate of the dimer of the relaxed structure just past the climax in the raising/lowering series was released and that structure was further optimized. If the geometry optimization led to either the global minimum or an intermediate local minimum, then the energy difference between the climax and the local minimum is taken as the barrier from this local minimum to either the global minimum or the intermediate local minimum. In some cases, the same procedure was used, but the fixed coordinate and scanning axis was  $x$  or  $y$  instead of  $z$ . In rare situations, linear interpolation of coordinates between a carbon atom of reactant structure and a carbon atom of product structure that are separated most significantly was used. In this approach, the carbon atom of reactant structure was moved along the corresponding virtual line with one coordinate ( $x$ ,  $y$  or  $z$ ) fixed during the geometry optimization of the series of interpolating points. If a climax was found and the point just past the climax relaxed to the product or to an intermediate local minimum after releasing the fixed coordinate, then the barrier was estimated as the energy difference between the climax and the reactant structure.

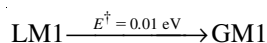
## 3. RESULTS AND DISCUSSION

In this section, results are presented from computational studies of carbon dimer adsorption onto the clean diamond C(110) surface. Global and local minima, as well as the transition states connecting them, are determined for the sequential adsorption of one, two or three carbon dimers onto the clean C(110) surface. An extensive effort was made to identify as many of the local minimum energy states as possible, with a primary focus on low-lying local minima and stabilized defect states. A defect is identified as any config-

uration separated from the global minima by thermally inaccessible kinetic barriers (or one that requires the traversal of a high energy pathway to reach the global minimum). This study assumes a thermally equilibrated room temperature environment, so kinetic barriers on the order of 0.5 eV or higher can be assumed to be inaccessible at temperatures at or near 300 K.

### 3.1. 1-Dimer Stationary Points (1-Dimer GM1)

The computation shows that if a carbon dimer is positionally deposited within a trough of a clean diamond C(110) surface, it relaxes to the global minimum structure easily. A single 1-dimer local minimum (LM1) structure was found which is 0.34 eV higher than the 1-dimer global minimum (GM1) in total energy. The energy barrier ( $E^\ddagger$ ) from the local minimum to the global one is only 0.01 eV:



The geometries of global and local minima shown in Figure 1 are in good agreement with the work of Sternberg et al.<sup>33</sup> However, their local minimum is 2.0 eV higher than the global minimum and has a barrier of 0.1 eV.

### 3.2. 2-Dimer Stationary Points (1-Dimer GM1 + 1 Dimer)

By positioning a second dimer around a 1-dimer global minimum and relaxing the structure, a global minimum (GM2) and 19 local minima (LM2) of 2-dimer carbon clusters were found. The potential energy of each structure is given in Table 1. Important pathways and barriers are summarized in Figure 2, and the structures of the global minimum and some local minima which are involved in high

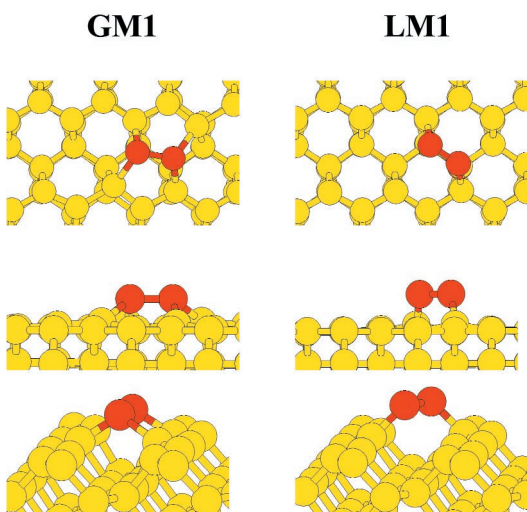
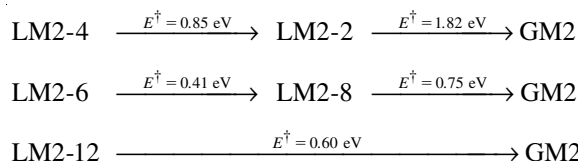


**Figure 1.** 1-dimer structure around GM1 on bare diamond C(110), top view and two side views.

**Table 1.** Potential energy of 2-dimer structures formed around GM1 on bare diamond C(110).

Stationary point	Potential energy (eV)
GM2	0.00
LM2-1	0.96
LM2-2	1.78
LM2-3	2.51
LM2-4	2.65
LM2-5	2.87
LM2-6	2.97
LM2-7	3.00
LM2-8	3.06
LM2-9	3.09
LM2-10	3.10
LM2-11	3.27
LM2-12	3.44
LM2-13	3.48
LM2-14	3.10
LM2-15	3.39
LM2-16	4.04
LM2-17	4.45
LM2-18	4.68

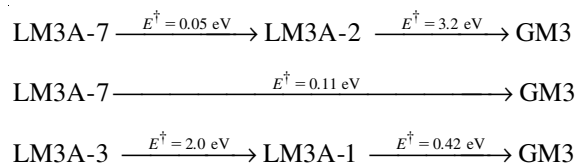
barriers are presented in Figure 3. The most important high barriers between LM2s and GM2 include:



Among the local minima, LM2-4 is the most intractable defect structure. In order to convert LM2-4 to the global minimum GM2, the structure must pass through two high barriers, 0.85 eV and 1.82 eV, respectively. LM2-6 and LM2-12 are also major defect structures to be avoided if GM2 is the desired target structure for C(110) surface growth.

### 3.3. 3-Dimer Stationary Points (2-Dimer GM2 + 1 Dimer)

By positioning a third dimer around a 2-dimer global minimum and relaxing the structure, a 3-dimer global minimum (GM3) and 17 local minima (LM3A) of 3-dimer carbon clusters were found. The potential energy of each structure is given in Table 2. Important pathways and barriers are summarized in Figure 4, and the structures of the global minimum and some local minima which are involved in high barriers are presented in Figure 5. The most important high barriers between LM3A's and GM3 include:



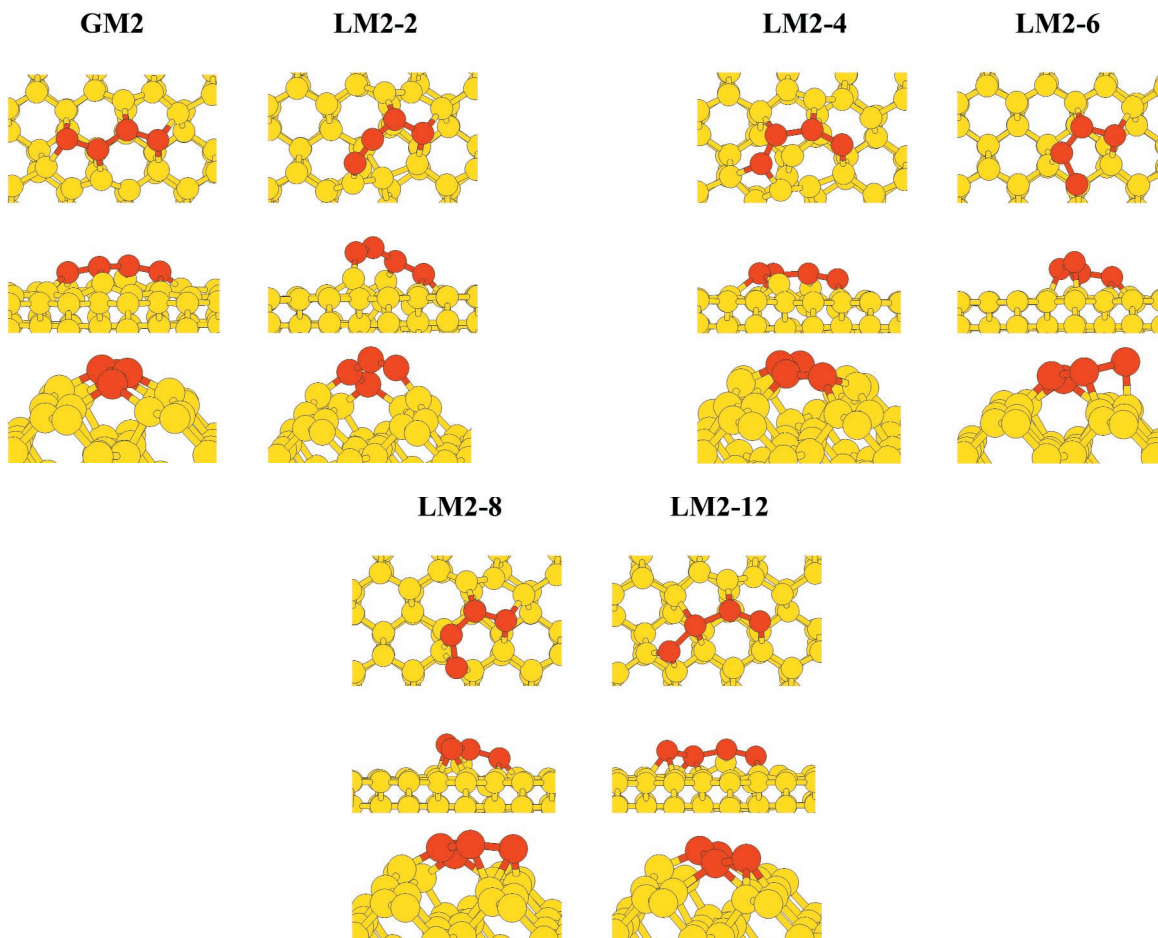
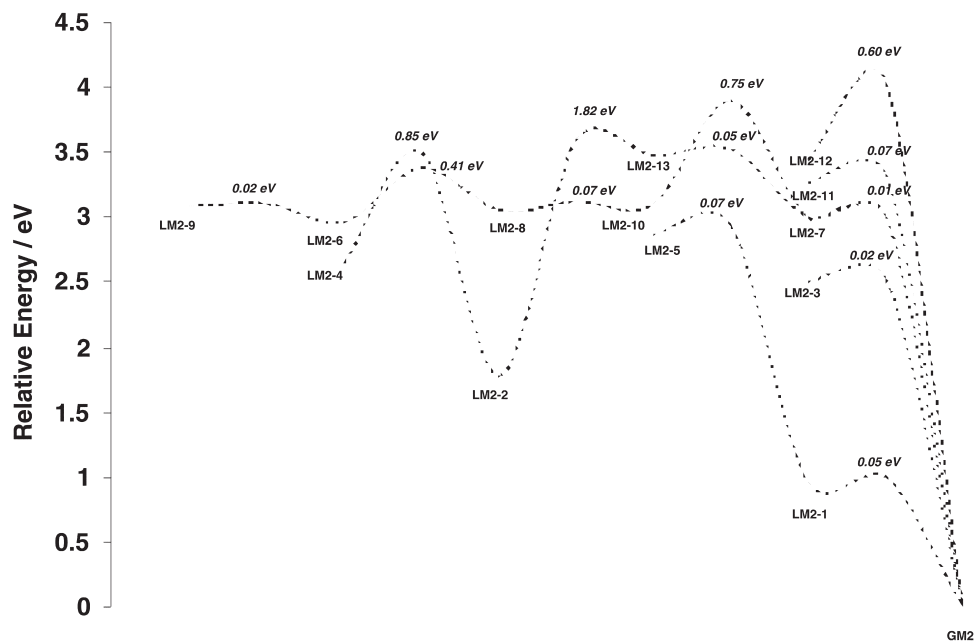
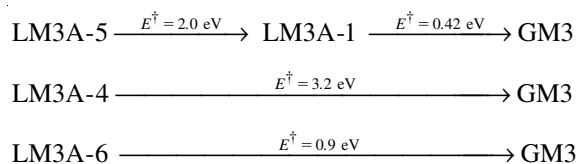


**Figure 3.** 2-dimer structures around GM2 on bare diamond C(110), top view and two side views.

**Table 2.** Potential energy of 3-dimer structures formed around GM2 on bare diamond C(110).

Stationary point	Potential energy (eV)
GM3	0.00
LM3A-1	0.19
LM3A-2	1.47
LM3A-3	2.19
LM3A-4	2.34
LM3A-5	3.06
LM3A-6	3.22
LM3A-7	3.32
LM3A-8	4.30
LM3A-9	4.49
LM3A-10	4.81
LM3A-11	4.83
LM3A-12	4.84
LM3A-13	5.04
LM3A-14	5.13
LM3A-15	5.37
LM3A-16	5.52
LM3A-17	7.71



There is one defect structure (LM3A-1) among the found local minima that could be converted to the 3-dimer global minimum (GM3) with a moderate barrier of 0.42 eV. Another local minimum (LMA-7) has only a small barrier of 0.11 eV to the 3-dimer global minimum. However, an even smaller barrier of 0.05 eV exists for the same local

minimum to an intermediate local minimum (LM3A-2), a defect structure that has a very large barrier of 3.2 eV against transition to the 3-dimer global minimum. LM3A-3, LM3A-4 and LM3A-5 are major defect structures to be avoided if GM3 is the desired target structure for C(110) surface growth.

### 3.4. 3-Dimer Stationary Points (2-Dimer LM2-4 + 1 Dimer)

Since the potential energy of the 2-dimer major defect structure LM2-4 is 2.65 eV, most of the 3-dimer local minima which were found by positioning a third carbon dimer around the LM2-4 local minimum are of higher potential. By positioning the third dimer around the 2-dimer LM2-4 local minimum and relaxing the structure, 18 local minima (LM3B) of 3-dimer carbon clusters were found. The potential energy of each structure is given in Table 3. Important pathways and barriers are summarized in Figure 6, and the structures of the global minimum and some local minima which are involved in high barriers are presented in Figure 7. The most important high barriers between LM3Bs and GM3 include:

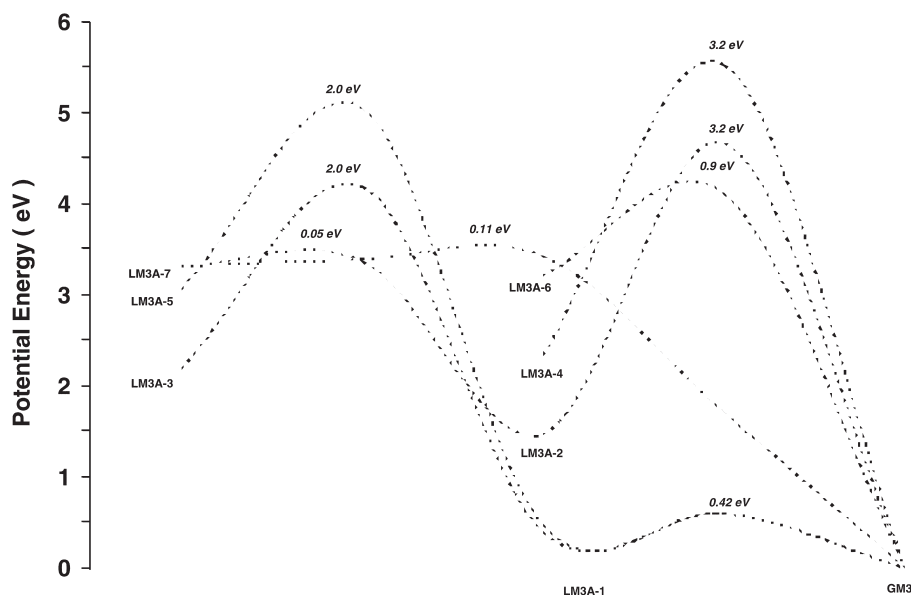
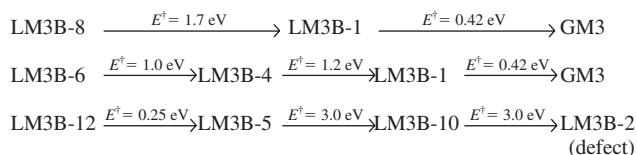


**Figure 4.** Potential energy diagram for 3-dimer stationary points formed around GM2 on bare diamond C(110).



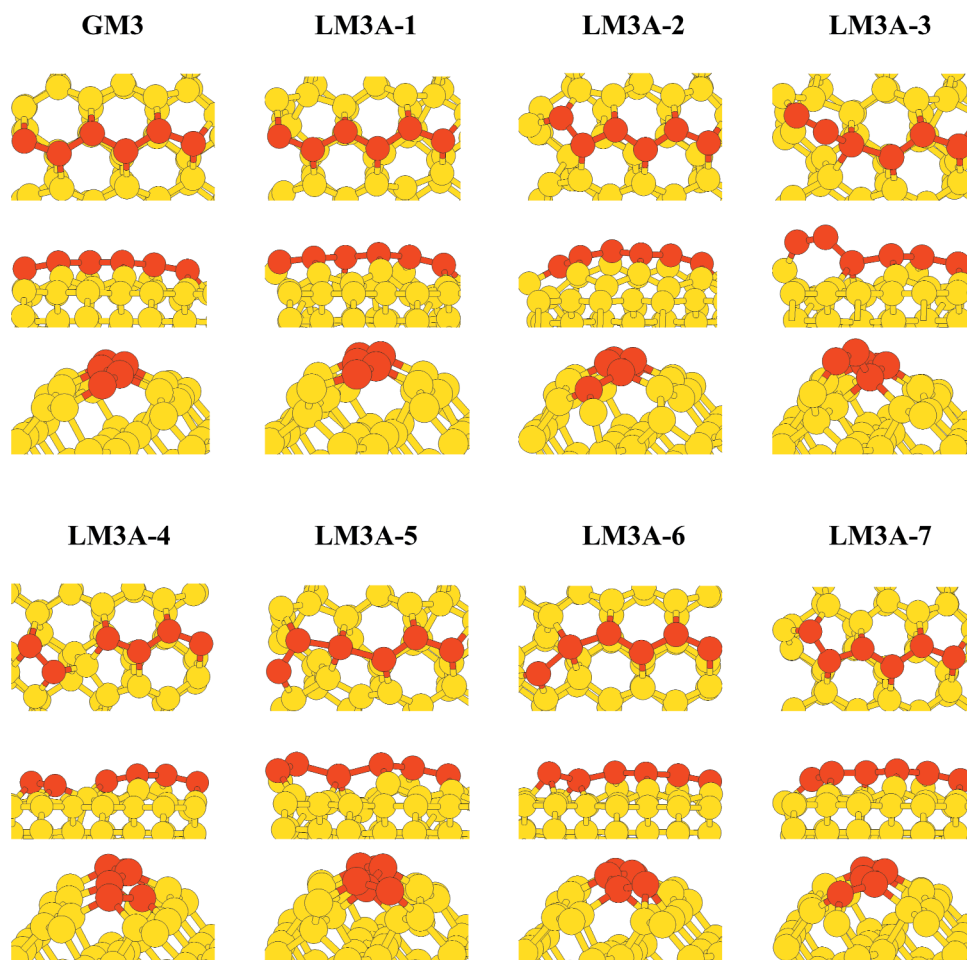
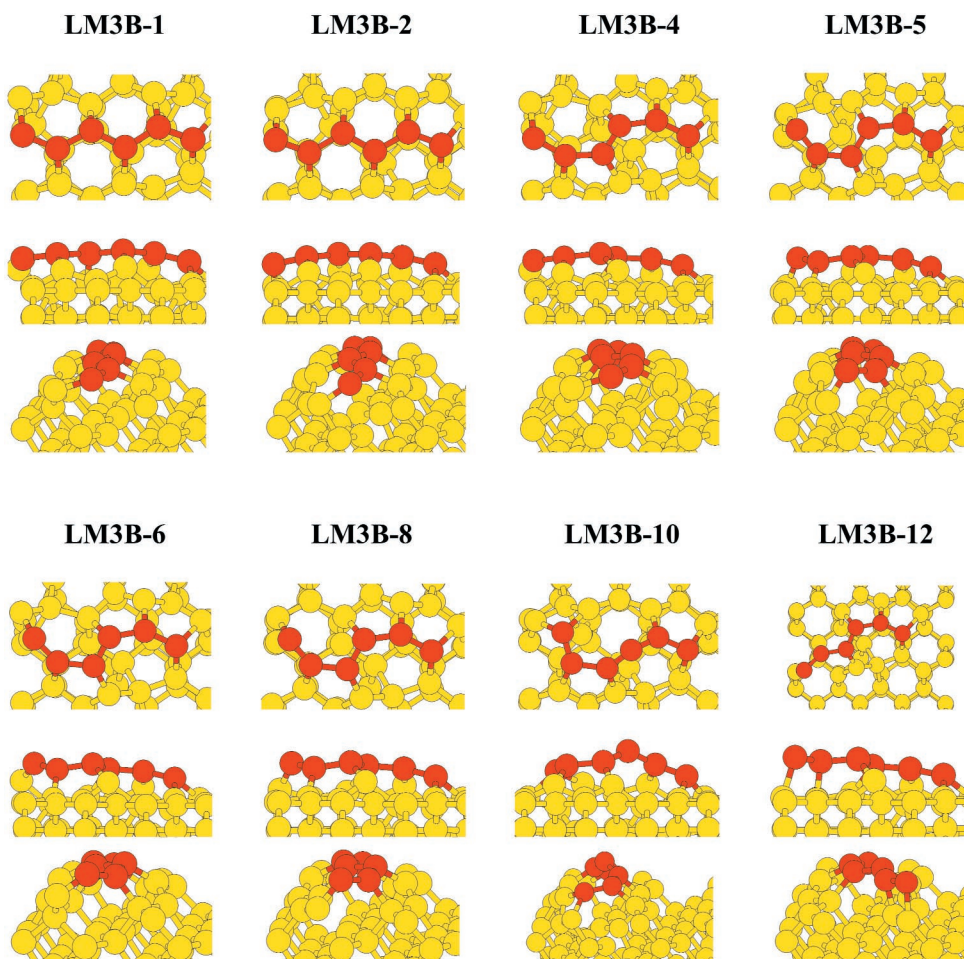
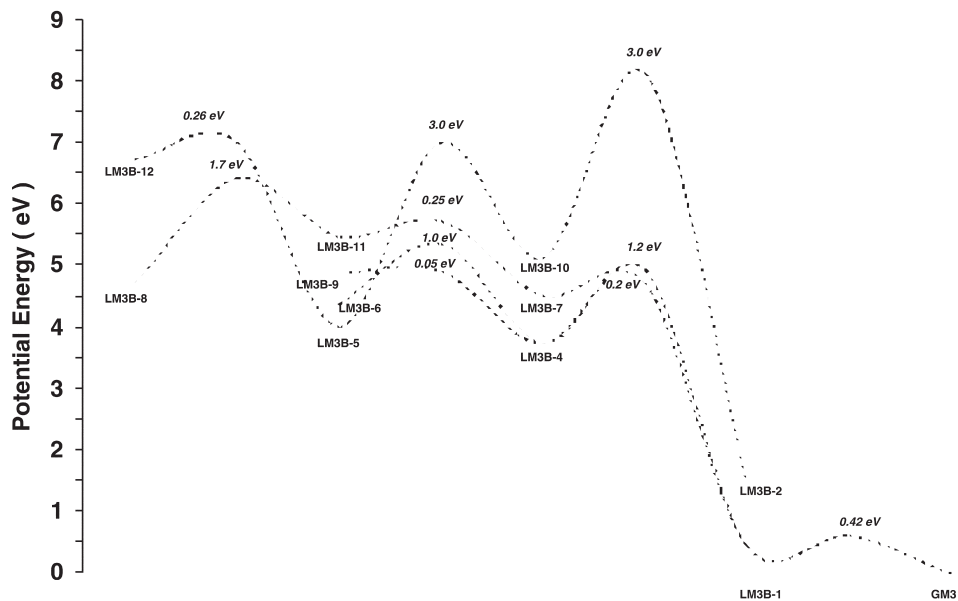


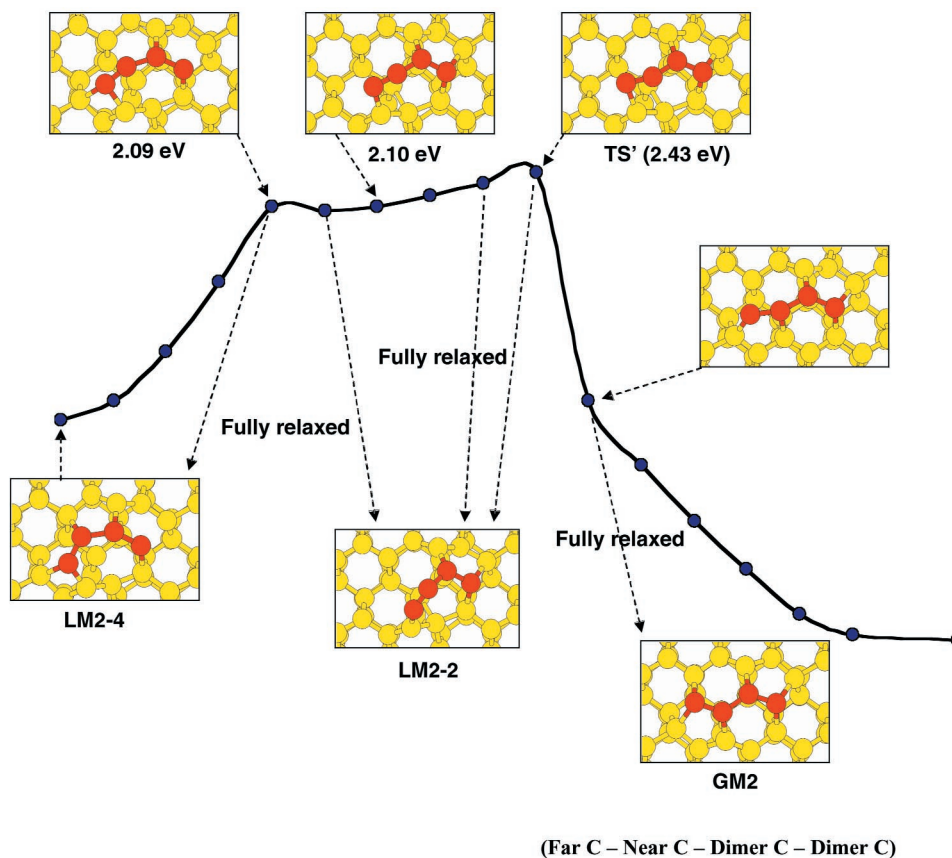
**Table 3.** Potential energy of 3-dimer structures formed around LM2-4 on bare diamond C(110).

Stationary point	Potential energy (eV)
GM3	0.00
LM3B-1	0.19
LM3B-2	1.49
LM3B-3	2.60
LM3B-4	3.73
LM3B-5	4.00
LM3B-6	4.36
LM3B-7	4.51
LM3B-8	4.71
LM3B-9	4.87
LM3B-10	5.12
LM3B-11	5.48
LM3B-12	6.74
LM3B-13	4.66
LM3B-14	6.19
LM3B-15	6.55
LM3B-16	8.19
LM3B-17	8.51
LM3B-18	8.56

### 3.5. Transition State between GM2 and High Barrier Local Minimum in Positional Placement Path

In order to simulate the positional placement of a  $C_2$  dimer, the transition state structure was searched by moving up the x coordinate of the near end of the second dimer, which is close to the 1-dimer global minimum, and moving down the x coordinate of the far end of the second dimer with steps of  $0.05 \text{ \AA}$  from the LM2-4 defect structure. Geometry optimization was performed at each point with x and z coordinates fixed, and full relaxations on some structures along the path were done. The scanned potential curve is shown in Figure 8 along with top views (xy plane) of relevant structures. This curve indicates that the first peak on the path from GM2 is the transition state (TS') to LM2-2. The distances projected on the xy plane of the far end and the near end between those structures are listed below the curve. These data show that the required positional placement accuracy for inserting a dimer at the desired global minimum (GM2) – avoiding the nearest transition state





Distances Projected on XY Plane of Far and Near Carbons of the Second Dimer:

Structure to Structure	Far C to Far C (Å)	Near C to Near C (Å)
GM2 $\rightarrow$ TS'	0.6587	0.5377
LM2-2 $\rightarrow$ TS'	1.0134	0.2024
GM2 $\rightarrow$ LM2-2	1.6700	0.8096

**Figure 8.** Scanned potential curve simulating the positional placement of  $C_2$  on bare diamond C(110), showing the path through transition state (TS') to defect structure LM2-4.

(TS') leading to an undesired defect – is 0.6587 Å and 0.5377 Å, measured from the first (“far”) or second (“near”) carbon atom, respectively, in the second added dimer.

### 3.6. Dimer Thermal Desorption and Surface Migration

The Arrhenius equation for the one-step thermal desorption rate  $k_1 = \nu \exp(-E_d/k_B T)$  may be used to crudely approximate the canonical residence time for a  $C_2$  dimer attached to a diamond surface heated to temperature  $T$ .<sup>42</sup> Taking  $T = 300$  K,  $k_B = 1.381 \times 10^{-23}$  J/K (Boltzmann's constant), desorption energy  $E_d > 8.0$  eV for diamond-bound dimers<sup>33, 42</sup> and the pre-exponential constant  $\nu \sim k_B T/h \sim 6 \times 10^{12} \text{ sec}^{-1}$  ( $h = 6.63 \times 10^{-34}$  J-sec) typi-

cally used for thermally-migrating chemisorbed hydrocarbon adatoms on diamond surface<sup>42</sup> (the precise value of which does not sensitively influence the conclusion), the lifetime of the  $C_2$  dimer against spontaneous dissociation from diamond surface is  $k_1^{-1} > 10^{121}$  sec at 300 K. The diffusion barriers to migration of  $C_2$  on clean C(110) diamond surface were calculated by Sternberg et al.<sup>33</sup> as 3.3–3.8 eV ( $k_1^{-1} = 10^{42} - 10^{51}$  sec at 300 K) along different crystallographic routes.

## 4. CONCLUSIONS

We have presented a computational and theoretical investigation of the gas-phase chemical vapor deposition growth and mechanosynthesis of clean diamond C(110) surfaces from carbon dimer precursors. Our theoretical re-



sults on the dimer-mediated growth chemistry of diamond C(110) are important to related experiments on the gas-phase growth of diamond C(110), but our conclusions focus on those results most relevant to the diamond positional mechanosynthesis proposal which is assessed in Part II:<sup>43</sup>

1. The adsorption of one C<sub>2</sub> dimer onto a hydrogen de-passivated diamond C(110) substrate leads to one of two local minima, one being the global minimum. The very low barrier of 0.01 eV separating the local from global minimum energy configuration is lower than k<sub>B</sub>T at room temperature, thereby lacking the ability to form stabilized surface defects from the adsorption of a single dimer. Thus, isolated dimers deposited on clean diamond C(110) at room temperature appear to be quite stable.
2. For the subsequent adsorption of a second carbon dimer in the close vicinity of the first, we identify 19 local minima in addition to the 2-dimer global minimum. Five of these local minimum energy structures require barriers greater than 0.5 eV to reach the global minimum, thereby constituting stabilized defects.
3. For the system involving three chemisorbed C<sub>2</sub> dimers, we identify 35 local minimum energy structures, ten of which are located in deep potential energy wells. The larger number of stable high-energy local minima suggests that the number of potential defects increases with system size (i.e., increases with the number of deposited carbon dimers) assuming the absence of long-range stabilizing factors.
4. Random clustering of carbon dimers onto the diamond substrate can produce many stable surface defects, ultimately forming graphitic or amorphitic regions. This suggests an isolated rather than clustered growth mechanism in conventional CVD, which is consistent with the low pressures required for gas-phase growth and with results from *ab initio* molecular dynamics (AIMD) simulations<sup>43</sup> not reported in this manuscript.

## References

1. J. C. Angus, A. Argoitia, R. Gat, Z. Li, M. Sunkara, L. Wang, and Y. Wang, in *Thin Film Diamond*, edited by A. Lettington and J. W. Steeds, Chapman and Hall, London (1994), p. 1.
2. H. Liu and D. S. Dandy, *Diamond Chemical Vapor Deposition: Nucleation and Early Growth Stages*, Noyes Publications, Park Ridge, NJ (1995).
3. D. N. Belton and S. J. Harris, in *Proceedings of the Second International Symposium on Diamond Materials*, edited by A. J. Purdes, J. C. Angus, R. F. Davis, B. M. Meyerson, K. E. Spear, and M. Yoder, The Electrochemical Society, Pennington, NJ (1991), p. 170.
4. C. A. Fox, G. D. Kubiak, M. T. Schulberg, and S. Hagstrom, in *Proceedings of the Third International Symposium on Diamond Materials*, edited by J. P. Dismukes and K. V. Ravi, The Electrochemical Society, Pennington, NJ (1993), p. 64.
5. M. S. Melnik, D. G. Goodwin, and W. A. Goddard, III, in *Mechanisms of Thin Film Evolution*, Symposium Volume 317, edited by Steven M. Yalisove, Carl V. Thompson, and David J. Eaglesham, Materials Research Society, Pittsburgh, PA (1994), p. 349.
6. D. R. Alfonso, D. A. Drabold, and S. E. Ulloa, *Phys. Rev. B* 51, 14669 (1995).
7. M. Nishitani-Gamo, K. Ping Loh, I. Sakaguchi, T. Takami, I. Kusunoki, and T. Ando, *J. Vac. Sci. Technol. A* 17, 2991 (1999).
8. M. W. Geis, H. I. Smith, J. Argoitia, J. Angus, G. H. Ma, J. T. Glass, J. Butler, J. Robinson, and R. Pryor, *Appl. Phys. Lett.* 52, 2043 (1988).
9. T. W. Mercer, J. N. Russell, Jr., and P. E. Pehrsson, *Surf. Sci.* 392, L21 (1997).
10. C. J. Chu, M. P. D'Evelyn, R. H. Hauge, and J. L. Margrave, *J. Appl. Phys.* 70, 1695 (1991).
11. C. H. Wild, N. Herres, and P. Koidl, *J. Appl. Phys.* 68, 973 (1990).
12. T. Tsuno, T. Tomikawa, S. Shikata, and N. Fujimori, *J. Appl. Phys.* 75, 1526 (1994).
13. C. Findeling-Dufour, A. Vignes, and A. Gicquel, *Diam. Rel. Mater.* 4, 429 (1995).
14. W. J. P. van Enkevort, G. Janssen, W. Vollenberg, J. J. Schermer, L. J. Giling, and M. Seal, *Diam. Rel. Mater.* 2, 997 (1993).
15. A. Badzian and T. Badzian, *Diam. Rel. Mater.* 2, 147 (1993).
16. T. L. McCormick, T. W. Mercer, G. Hubler, and J. E. Butler, in *Proceedings of the 1996 Diamond Conference*, Cambridge, UK (1996), p. 8.1.
17. K. Kobashi, K. Nishimura, K. Miyata, K. Kumagi, and A. Nakaue, *J. Mater. Res.* 5, 2469 (1996).
18. C. C. Battaile, D. J. Srolovitz, and J. E. Butler, *J. Appl. Phys.* 82, 6293 (1997).
19. C. C. Battaile, D. J. Srolovitz, and J. E. Butler, *Diam. Rel. Mater.* 6, 1198 (1997).
20. C. C. Battaile, D. J. Srolovitz, and J. E. Butler, *J. Cryst. Growth* 194, 353 (1998).
21. C. C. Battaile, D. J. Srolovitz, I. I. Oleinik, D. G. Pettifor, A. P. Sutton, S. J. Harris, and J. E. Butler, *J. Chem. Phys.* 111, 4291 (1999).
22. M. P. D'Evelyn, C. J. Chu, R. H. Hauge, and J. L. Margrave, *J. Appl. Phys.* 71, 1528 (1992).
23. C. E. Johnson, W. A. Weimer, and F. M. Cerio, *J. Mater. Res.* 7, 1427 (1992).
24. M. P. D'Evelyn, J. D. Graham, and L. R. Martin, *Diam. Rel. Mater.* 10, 1627 (2000).
25. D. Huang, M. Frenklach, and M. Maroncelli, *J. Phys. Chem.* 92, 6379 (1988).
26. M. Frenklach and H. Wang, *Phys. Rev. B* 43, 1520 (1991).
27. J. Peploski, D. L. Thompson, and L. M. Raff, *J. Phys. Chem.* 96, 8538 (1992).
28. D. N. Belton and S. J. Harris, *J. Chem. Phys.* 96, 2371 (1992).
29. D. A. Horner, L. A. Curtiss, and D. M. Gruen, *Chem. Phys. Lett.* 233, 243 (1995).
30. P. C. Redfern, D. A. Horner, L. A. Curtiss, and D. M. Gruen, *J. Phys. Chem.* 100, 11654 (1996).
31. R. Astala, M. Kaukonen, R. M. Nieminen, G. Jungnickel, and Th. Frauenheim, *Phys. Rev. B* 63, 91402 (2001).
32. D. M. Gruen, P. C. Redfern, D. A. Horner, P. Zapol, and L. A. Curtiss, *J. Phys. Chem. B* 103, 5459 (1999).
33. M. Sternberg, M. Kaukonen, R. M. Nieminen, and Th. Frauenheim, *Phys. Rev. B* 63, 165414 (2001).
34. D. M. Gruen, S. Liu, A. R. Krauss, J. Luo, and X. Pan, *J. Appl. Phys.* 64, 1502 (1994).
35. C. J. Chu, R. H. Hauge, J. L. Margrave, and M. P. D'Evelyn, *Appl. Phys. Lett.* 61, 1393 (1992).
36. K. C. Pandey, *Phys. Rev. B* 25, 4338 (1982).
37. A. V. Hamza, G. D. Kubiak, and R. H. Stulen, *Surf. Sci.* 237, 35 (1990).
38. P. G. Lurie and J. M. Wilson, *Surf. Sci.* 65, 453 (1977).

39. B. N. Davidson and W. E. Pickett, *Phys. Rev. B* 49, 11253 (1994).
40. G. Kern and J. Hafner, *Phys. Rev. B* 56, 4203 (1997).
41. F. Maier, R. Graupner, M. Hollering, L. Hammer, J. Ristein, and L. Ley, *Surf. Sci.* 443, 177 (1999).
42. R. C. Merkle and R. A. Freitas Jr., *J. Nanosci. Nanotechnol.* 3, 319 (2003).
43. D. J. Mann, J. Peng, R. A. Freitas Jr., and R. C. Merkle, *J. Comput. Theor. Nanosci.* 1, 71 (2004).
44. G. Kresse and J. Furthmuller, *Vienna Ab-initio Simulation Package (VASP): The Guide*, VASP Group, Institut für Materialphysik, Universität Wien, Sensengasse 8, A-1130 Wien, Vienna, Austria (2003).

Received: 2 October 2003. Revised/Accepted: 16 October 2003.